Resonant properties of the memory capacity of a laser-based reservoir computer with filtered optoelectronic feedback

Gleb Danilenko, Anton Kovalev, Evgeny Viktorov, Alexandre Locquet, David S. Citrin, Damien Rontani

Resonant properties of the memory capacity of a laser-based reservoir computer with filtered optoelectronic feedback

G.O. Danilenko,[1, a)] A. V. Kovalev,[1, a)] E. A. Viktorov,[1] A. Locquet,[2, 3] D. S. Citrin,[2, 3] and D. Rontani[4]
[1)] *ITMO University, 199034 Saint Petersburg, Russia*
[2)] *Georgia Tech-CNRS IRL 2958, Georgia Tech-Europe, 57070 Metz, France*
[3)] *School of Electrical and Computer Engineering, Georgia Institute of Technology, Atlanta, GA 30332, USA*
[4)] *Chair in Photonics, LMOPS UR 4423 Laboratory, CentraleSupélec & Université de Lorraine, 57070 Metz, France*

(*Electronic mail: danilenko.gleb98@gmail.com)

(Dated: 14 September 2023)

We provide a comprehensive analysis of the resonant property of the memory capacity of a time-delay reservoir computer based on a semiconductor laser subjected to filtered optoelectronic feedback. Our analysis reveals first how the memory capacity decreases sharply when the input-data clock cycle is slightly time-shifted from the time delay and its multiples. We attribute this effect to the inertial properties of the laser. We also report on the dampening of the memory-capacity drop at resonance with a decrease of the virtual node density and its broadening with filtering properties of the optoelectronic feedback. These results are interpretated using the eigenspectrum of the reservoir obtained from a linear stability analysis. Then, we unveil an invariance in the minimum value of the memory capacity at resonance with respect to a variation of the number of nodes if the number is big enough and quantify how the filtering properties impact the system memory in and out of resonance.

A reservoir computer carries out physics-based computing in which the computation is realized in the nonlinear dynamics of the system. Reservoir computers are a subclass of recurrent neural networks, but benefit from simplified training compared with the larger class of recurrent neural networks by only regressing a subset of hyperparameters associated to the network's output layer. One type of reservoir computer is realized by a nonlinear system (node) with the time-delay feedback loop; the state of the dynamical variables in the feedback loop at a set of time intervals constitute virtual nodes of the reservoir computer. It is important therefore to understand how the physically realized reservoir computer affects its performance. Here we investigate the performance of a time-delay reservoir computer composed of a laser diode with an optoelectronic feedback loop. The laser is a nonlinear device that is characterized by its ability to demonstrate a variety of dynamical regimes when subjected to the optoelectronic feedback, *i.e.*, when its emission intensity signal is added to or subtracted from its pump current. The optoelectronic signal conversion inherently has a limited bandwidth, and we analyze how it affects frequencies of the system's small-signal response that is crucial for the reservoir computing system. We find that the reservoir computer performance is severely degraded when the symbol input rate is in resonance with the difference between adjacent frequencies of the response as the reservoir's ability to remember (memory capacity) input at past times is strongly reduced. We show that decreasing the filter bandwidth introduces inertia to the response and dispersive spread of the frequencies thus affecting the position and width of the resonance. An analysis of the memory capacity of the time-delay reservoir computer based on the laser diode with optoelectronic feedback reveals the persistence of minimal connectivity as well as inertial and dispersion properties and provides guidance to attain high performance.

I. INTRODUCTION

Recent developments in artificial neural networks (ANNs) have enabled the emergence of novel computing paradigms to solve highly demanding tasks in data analysis and processing[1]. Recurrent neural networks (RNNs) are particularly suited for tackling time-dependent tasks and big-data analysis. One of *caveat* is the complexity of training of RNNs when compared to feedforward networks[2]. Reservoir computing (RC) simplifies the training of RNNs by only regressing a subset of hyper-parameters associated to the RNN's output layer. As a result, RC can be trained using simple linear (or ridge) regression[3], on a reduced set of tunable parameters. Various physical implementations of RC have been proposed[4,5], from water buckets[6] to mechanical oscillators[7], spintronic systems[8], and micro-electronics with field programmable gate arrays (FPGAs)[9], to name a few). Amongst the various approaches that have been considered, photonics-based RCs are attractive because of their high energy efficiency and large data processing bandwidth[10–12]. Successful experimental demonstration of photonic RCs have been performed with optoelectronic oscillators[13–15], semiconductors lasers with optical feedback[16,17], photonic integrated circuits[18–20], and free-space optical setups[21–23].

A subset of photonic RCs is known as time-delay RCs (TDRCs), which rely on time-multiplexing the recurrent-

[a)] These authors contributed equally to this work

network structure by considering virtual neurons temporally distributed within the feedback loop delay time. The network connectivity is induced by the so-called *masking procedure*: It is a preprocessing stage, where input data is modulated by a fast-oscillating, periodic signal (the mask) with a time period generally corresponding to the propagation time of signals in the feedback loop. This was originally proposed by Appeltant and coworkers in their seminal work[24]. The main advantage of TDRC is its simplified structure that requires the use of a single physical node. However, it usually leads to slower information-processing speed compared with spatially-extended systems. Numerous photonic implementations of the TDRC approach have been proposed, including those with optoelectronic oscillators with delayed feedback[25,26], with edge-emitting semiconductor lasers (EELs) with optical feedback[16] or with optoelectronic feedback[27], with vertical-cavity surface-emitting lasers (VCSELs) with optical feedback[28,29], with semiconductor ring lasers[30] and with photonic integrated circuits with integrated feedback[19,31]. Photonic TDRC has shown state-of-the-art performance on various tasks such as nonlinear channel equalization and spoken-digit recognition[16,25,32].

As nonlinear time-delay systems, TDRC architectures can display so-called *resonant effects*, which may significantly affect their performance. One of these resonant phenomena exists between the input clock-cycle time T_{cc} (*i.e.*, the time period of the masking signal) and the delay time τ associated with signal propagation in the feedback loop (time delay τ). One of the measurable consequences of this resonance effect is a reduction of the memory capacity (*MC*) of the TDRC, a task-independent metric measuring the ability of the TDRC to reconstruct past input from current state values[33], when T_{cc} and τ are similar in value. This effect has already been documented in TDRC configurations based on EELs with optical feedback[34–37]. Reduced performance has also been reported for higher-order resonances, (*i.e.,* $a\tau \approx bT_{cc}$ with a and b natural numbers)[35,36]. Based on the spectral analysis of the system's dynamics, Köster *et al.* suggested that for efficient TDRC performance, the product of the imaginary part of an eigenvalue with the input clock cycle, should be different from $k\pi$ with k an integer to avoid half circle rotations during one input time[38].

In recent work on a TDRC based on a laser diode subjected to optoelectronic feedback[27], we have shown that tailoring the filtering properties of the feedback has a significant impact on the MC of the system while preserving its computational ability[39]. This suggests filtering could have a nontrivial effect on the resonant properties of photonic TDRCs.

In the present work, we provide a detailed analysis of the resonance properties of the MC of a TDRC based on a laser diode with filtered optoelectronic feedback. The manuscript is organized as follows: In Sec. II, we detail the numerical model of the laser with delayed, filtered, optoelectronic feedback. In Sec. III, we will provide a detail study of the *MC* properties and the impact of key physical parameters such as the number of nodes and the feedback parameters. We base our analysis on the eigenvalue spectrum of the linearized model about its only non-trivial equilibrium point of the TDRC. The use of an eigenvalue analysis allows us to highlight and report on the existence of an inertial offset in the clock cycle value leading to the resonance, an invariance of the minimum MC at resonance, and, second, the possible changing of resonance with respect to physical properties of the feedback. In Sec. IV we present our conclusions.

II. MODEL

We consider a delay differential equation (DDE) model for a semiconductor laser subject to a bandpass-filtered optoelectronic feedback[39]:

$$\dot{I}(t) = 2N(t)I(t), \tag{1}$$

$$\dot{I}_{FH}(t) = -{\tau_H}^{-1} I_{FH}(t) + \dot{I}(t), \tag{2}$$

$$\dot{I}_{FL}(t) = -{\tau_L}^{-1}[I_{FL}(t) - I_{FH}(t)], \tag{3}$$

$$\begin{aligned}\varepsilon^{-1}\dot{N}(t) = {} & P[1+\xi M_f(t)] + \eta I_{FL}(t-\tau) - N(t) \\ & -[1+2N(t)]I(t),\end{aligned} \tag{4}$$

where $I(t)$ is the normalized intensity of the laser field; $N(t)$ is the carrier density; $I_{FH}(t)$ is the high-pass filtered intensity signal and τ_H is the inverse of the high-pass filter cut-off frequency; $I_{FL}(t)$ is the low-pass filtered intensity signal and τ_L the inverse of the low-pass filter cut-off frequency; P is the pump-above-the-threshold parameter, defined as $P = (J - J_{thr})/2$, with a modulation function $M_f(t)$ for the masked input data and maximum modulation amplitude ξP; η is the feedback strength (either positive or negative);τ is the feedback delay time; and ε is the ratio of the photon to the carrier lifetimes.

A modulation function $M_f(t)$ describes an input signal S multiplied by a T_{cc}-periodic mask $M(t)$, which is piecewise-constant on the inter-delay interval $\theta = T_{cc}/N$, where N is the number of virtual nodes, and T_{cc} is the clock cycle. See Ref. 27 for details. The mask values are random numbers uniformly distributed in $[-1, 1]$.

We consider the following set of experimentally relevant parameters according to Ref. 40 for further numerical analysis: $\varepsilon = 0.1$, $\tau_H = 2000$, $\tau = 1000$, and $\xi = 0.1$. Time parameters are measured in the units of the photon lifetime $t_p = 10$ ps.

III. RESONANT PROPERTIES OF THE MEMORY CAPACITY

We analyze the effect on *MC* defined in Eq. (5) below, when the clock cycle T_{cc} is approximately equal to the delay time τ, for a photonic RC with optoelectronic feedback (see Fig.1). We numerically investigate the impact of key tunable parameters of the reservoir, such as the number of nodes N and low-pass-filter cut-off frequency τ_L^{-1} on the appearance, location, and minimum value of the *MC* resonance. The *MC* is a metric that characterizes the ability of a RC to reconstruct the previous inputs from its current state vector. It is mathematically

defined as[41]:

$$MC = \sum_{d=1}^{\infty} mc_d = \sum_{d=1}^{\infty} \frac{\mathrm{cov}^2(O_i, S_{i-d})}{\sigma^2(S_i)\sigma^2(O_i)}, \tag{5}$$

where mc_d is called a memory function, σ^2 is the variance, cov is the covariance, O_i is the output data value at the i-th input step (corresponding to the input of one symbol during a period T_{cc}), S_{i-d} is the input data value delayed by d input steps. The memory function mc_d characterizes how well the output of the reservoir, that is trained to restore the input that occurred d inputs before, correlates with the aforementioned input. Numerically, the maximum calculated depth d was chosen to be 500, and we took only values $mc_d \geq 0.01$ for the sum in Eq. 5.

Further, we examine the memory functions to specify their connection to the resonance effect, provide the eigenvalue spectrum analysis determining the resonance location, and explain the impact of the dispersive spread of the eigenfrequencies on the resonance width.

A. Node density and memory profiles

In this section, we analyze the impact of the number of nodes on the *MC* resonance. It is known that *MC* scales with the number of nodes in a RC, with the upper-bound being the network size[33,42]. In the case of time-delay based RCs, the inter-delay θ controls the local connectivity between neighboring virtual neurons with an evanescent coupling kernel, so that a quasi-disconnected network is achievable if θ is large with respect to the the typical response time of the physical node[41].

Considering a fixed time delay τ while changing the number N of virtual nodes will result in a change in the virtual-node density, and hence in the strength of the connectivity between nodes. Here, we change T_{cc} for a constant N modifying the inter-delay θ and time during which the input symbol is fed into reservoir. Figure 1 shows the dependence of *MC* on the clock cycle T_{cc} for various numbers N of nodes. When the number of node exceeds $N > 70$, we observe a saturation of the *MC* at an average value ~ 35 with a drop at the resonance leading to $MC(T_{cc} \approx \tau) \sim 10$. This saturation may originate in a large density of virtual nodes that imposes highly correlated input-output responses, thus strongly limiting the contribution of additional nodes beyond $N = 70$ in the overall *MC* of the TDRC with filtered optoelectronic feedback.

Another salient feature is the persistent minimum value of *MC* at the resonance and its steady location for the fixed parameters of the reservoir. However, the resonant effect is attenuated if the number of nodes N is below the minimum value of the *MC* (around 10), as shown in Fig. 1. Indeed, even though there is a drop at the same position, its magnitude is comparable with *MC* fluctuations within the full T_{cc} range $[0.9\tau, 1.1\tau]$, so it is less clear that the drop is caused by the resonance effect. Of note, in Fig. 1 *MC* is shown only for positive feedback sign; nevertheless, its minimum value and its location do not depend on the feedback sign and remain the same.

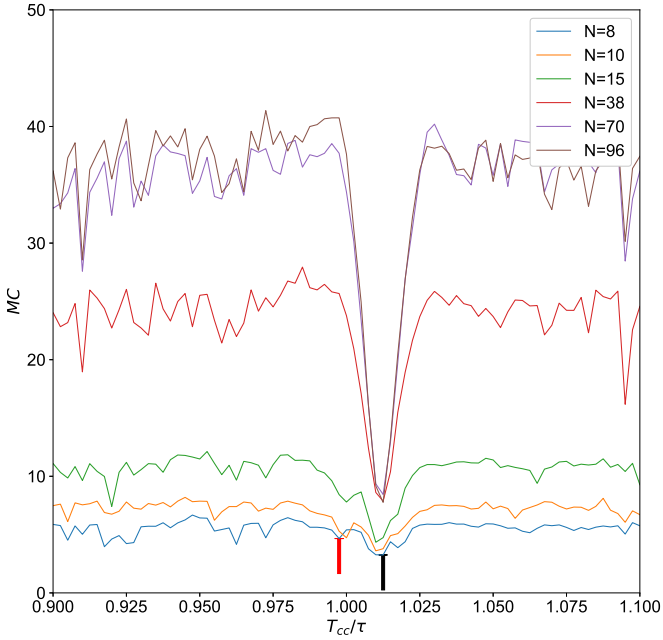

FIG. 1. *MC* versus clock cycle T_{cc} for various numbers N of nodes. Black and red marks provide the reference for the resonant and off-resonant position for further discussion, correspondingly. $P = 0.2$, $\tau_L = 7.5$, $\eta = 0.98$. The other parameters are given in the text.

In order to gain insight into the system behavior in and out of the resonance, the memory functions mc_d are plotted in Fig. 2. For more details about the memory function see Ref. 24. The memory profiles are very different, for different values of N, for nonresonant cases [panels (a), (c), (e)], but remain nearly the same for the resonant cases at any N, showing an initial fast decay, corresponding to a decreased *MC*, followed by a slow decay stage. A possible explanation of such behavior of the memory function is that fast decay of the memory profile is associated with a topological change the RC's connectivity at the resonance: the resonance breaks the propagation of the delayed signal from one virtual node to another.

The slope of the slow stage at the resonant cases [Fig. 2(d) and (f)] is the same as the slope of the decaying memory profile at the non-resonant cases [Fig. 2(c) and (e)], illustrating the persistence of the connectivity except the loss of connections which correspond to the fast decay of the memory profile. Invariance of the memory profile with respect to N results in the persistence of the minimum *MC* for the resonant cases. The resonance effect is not pronounced for a small number of nodes ($N = 8$, 10) as the memory profile decays very slowly and the mc_d values are very small for the both resonant and non-resonant cases.

B. Eigenspectrum analysis for inertia, dispersion, and filtering

The low-pass filtering of the feedback signal affects the RC performance[39], but its impact on the MC is different within or

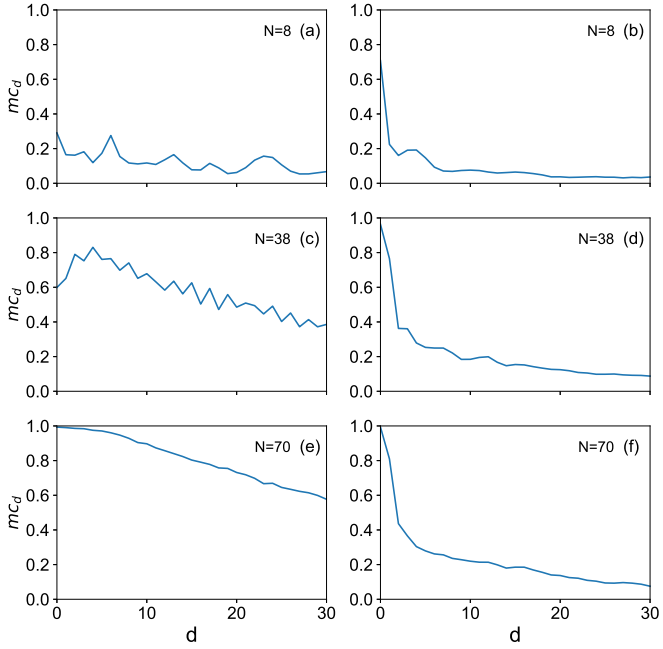

FIG. 2. Memory function mc_d for various numbers N of nodes for the T_{cc} values denoted by red and blue arrows in Fig. 1 corresponding to the cases of (a), (c), (e) out of resonance and (b), (d), (f) on resonance. The number of nodes: (a), (b) N = 8, (c), (d) N = 38, (e), (f) N = 70. The other parameters are the same as in Fig. 1.

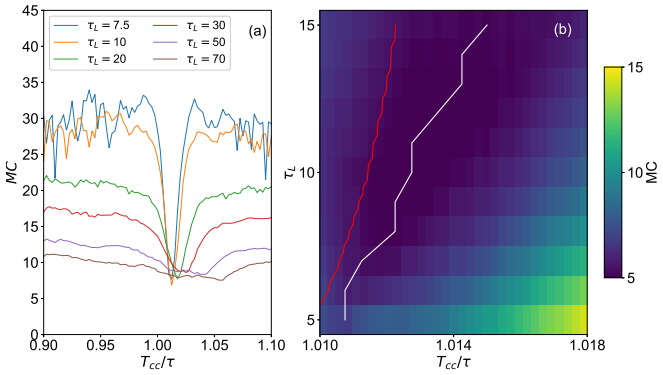

FIG. 3. (a) MC versus clock cycle T_{cc} for various values of τ_L with $P = 0.2$ and $\eta = 0.98$. (b) diagram of MC in (τ_L,T_{cc}) plane with $P = 0.4$, η = 0.6. The red line represents the calculated resonance's location and its shifting with τ_L using the spectral analysis that is defined as the inverse of the mean eigenvalue interval $1/\overline{D_1}$. The white line is the minimum MC.

outside of the resonance. In non-resonant cases, MC decreases with reduced fluctuations levels as is observed in Fig. 3(a). Moreover, the resonance becomes wider, leading eventually to a nearly flat MC profile without pronounced resonance.

To gain insight into why this happens, we perform a linear stability analysis of the system for the non-trivial steady-state $I(t) = P$, $I_{FL}(t) = I_{FH}(t) = 0$, $N(t) = 0$, for which the characteristic equation reads (see also Ref. 39):

$$[2\varepsilon P(1+\lambda)+\lambda(\varepsilon+\lambda)](1+\tau_H\lambda)(1+\tau_L\lambda) \\ -2e^{-\lambda\tau}\eta\varepsilon P\lambda\tau_H = 0, \quad (6)$$

where λ is an eigenvalue of the linearization of Eqs. (1)–(4) about the non-trivial steady-state of interest and describes the small-signal response of the system to the input signal.

The calculated eigenvalue spectra are given in Fig. 4(a). Particularly, we are interested in the imaginary parts of the eigenvalues $\mathrm{Im}(\lambda)$, or eigenfrequencies, that characterize the frequencies of the system's response to perturbations and, therefore, characterize MC[39]. As τ_L increases, the eigenvalue spectrum transforms and its shape becomes narrower meaning increased damping of the eigenfrequencies less than $1/\tau_L^{-1}$. Furthermore, we have shown in a previous study[39] the existence of a dependence of MC on the flatness and proximity of the eigenvalue spectrum to the imaginary axis. As a result, MC is reduced out of resonance [Fig. 3(a)] because a smaller number of eigenvalues is in proximity to the imaginary axis.

The bandwidth limitation of the feedback has a significant effect on the eigenvalue spectrum, and may result in completely filtering out the feedback signal at the frequencies corresponding to the modulational instability, *i.e.*, undamping of the laser's relaxation oscillations (see Ref. 39 for details), as occurs for $\tau_L = 30$ and $\tau_L = 70$ in Fig. 4(a). In this case, only a few eigenvalues contribute to the system's response, and the timescales associated with the laser are not manifested in the dynamics of the system, so the instabilities can be characterized only by feedback-related timescales (*i.e.* τ and bandpass filter cut-off frequencies τ_L^{-1} and τ_H^{-1}).

The eigenvalue spectrum analysis can provide further insight about the typical scaling of the MC with respect to the filtering characteristic of the feedback at the resonance. Based on the spectral analysis, we introduce two quantities D_1 and D_2 that characterize the distribution of the eigenvalues. We find that the inverse of the mean difference between adjacent eigenfrequencies provides a good estimation of the scaling of the resonant clock cycle T_{cc} value. The normalized interval between two adjacent eigenfrequencies is defined as

$$D_1(i) = \frac{\mathrm{Im}(\lambda_{i+1}) - \mathrm{Im}(\lambda_i)}{2\pi}\tau, \quad (7)$$

where $i \geq 0$ is the eigenvalue number, and the eigenvalues are numbered according to increasing $\mathrm{Im}(\lambda_i)$. We take only the positive part of the eigenvalue spectrum for the analysis due to its symmetry with respect to the real axis[39].

In our system, $D_1(i)$ deviates significantly from unity [see Fig. 4(b)] due to filtering. This is drastically different from the case described in Refs. 35 and 38 where $\mathrm{Im}(\lambda) \approx \pi K/\tau$ with $K \in \mathbb{Z}$. In the following we relate the variation of the resonance's properties to the inertia and dispersion imposed by the filtering.

Figure 3(b) shows the position of the resonant dip and the inverse of the mean eigenfrequency interval $1/\overline{D_1}$, both shifting to higher values when τ_L increases. The mean eigenfre-

quency interval is defined as

$$\overline{D_1} = \frac{1}{C} \sum_{\substack{j\geq 0: \\ \mathrm{Re}(\lambda_j)\tau \geq -2}} D_1(j), \tag{8}$$

where C is the number of eigenvalues having a real part satisfying $\mathrm{Re}(\lambda_j)\tau \geq -2$, *i.e.*, the averaging goes over eigenvalues that are not strongly damped. If we consider the reservoir as an ensemble of coupled oscillators at different eigenfrequencies driven by the reservoir's input, the quantity $\overline{D_1}$ characterizes the mean frequency spacing between them. In our active nonlinear time-delayed system, the decrease of $\overline{D_1}$ manifests the effect of inertia when the feedback loop bandwidth is shrinking, and the system dynamics is mainly determined by the feedback as the laser timescales are significantly damped.

By inertia here we understand the effect of the increase of the characteristic response time in a dynamical system with respect to τ. This effect is an inherent feature of time-delayed dynamical systems and is associated with information propagation and causality (see, e.g., Ref. 43). In our system, the effect is enhanced because of the presence of filtering in the feedback loop. The effect of filtering on the characteristic time-scale was previously studied in lasers with feedback, e.g., it was shown that decreasing the optical filter bandwidth leads to the decrease of the spacing between external cavity modes of a semiconductor laser with delayed optical feedback[44].

In our system, $1/\overline{D_1} > \tau$ which also highlights that the resonant value of T_{cc} is determined by the interval between eigenfrequencies accounting for the inertial effect, and therefore can be different from τ.

Further, apart from the shift, the resonant dip also becomes broader for large values of τ_L [Fig. 3(a)]. If we, again, consider the reservoir as an ensemble of oscillators, this broadening is determined by the dispersive spread of the eigenvalues, which forms their non-equidistant character. To illustrate this and to characterize the dispersive spread of the eigenfrequencies, we compute the differences between the adjacent eigenfrequency intervals as

$$\begin{aligned} D_2(i) &= [D_1(i+1) - D_1(i)]\tau = \\ &= (\mathrm{Im}(\lambda_{i+2}) - 2\mathrm{Im}(\lambda_{i+1}) + \mathrm{Im}(\lambda_i))\tau^2/(2\pi), \end{aligned} \tag{9}$$

that is reminiscent of a numerical second derivative definition, and also optical dispersion.

It is seen in Fig. 4(c) that increasing τ_L results in an enhancement of the non-equidistance between eigenfrequencies. Equidistant eigenfrequencies define the location of a unique resonance, but multiple non-equidistant eigenfrequencies generate multiple resonant drops slightly shifted from each other. These drops coalesce in a single broaden drop.

C. Intensity patterns and connectivity

To illustrate the reservoir behavior inside and outside the resonance, as well as connections between virtual nodes, $2D$ diagrams (Figs. 5, 6), in the spirit of the spatio-temporal representation of delay systems proposed in Ref. 45, are presented.

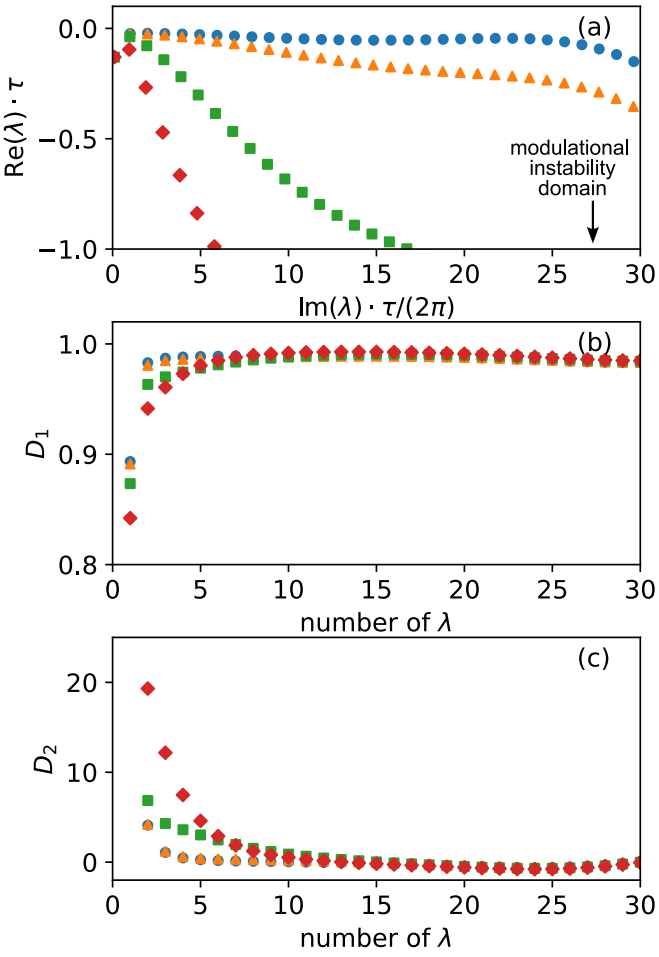

FIG. 4. Eigenvalue analysis: (a) the numerically computed eigenvalues of the linearized system of Eqs. (1)–(4); (b) the intervals $D_1(i)$ between the adjacent eigenfrequencies, according to Eq. 7; (b) differences of the adjacent eigenfrequency intervals D_2 (Eq. 9) showing their non-equidistant character. Color shows the low-pass filter timescale: $\tau_L = 7.5$ (blue), $\tau_L = 10$ (orange), $\tau_L = 30$ (green), and $\tau_L = 70$ (red). The other parameters are the same as in Fig. 3.

The diagrams are constructed as follows: the intensity time-trace is split into intervals having a length equal to T_{cc}, and successive slices are stacked in the vertical direction resulting in the two-dimensional plot. This representation shows the dynamic reservoir development within one clock cycle, for a total of 100 cycles. Figure 5 illustrates that information is diffused across non-neighboring virtual nodes, in the non-resonant cases [diagonal lines in Figs. 5(a) and (c)], while it remains localized to specific positions in time [vertical lines in Figs. 5(b) and (d)], in the resonant cases. This could explain the reduced MC with resonant conditions. Of note, the number of vertical lines is larger in Fig. 5(d) compared with Fig. 5(b), since in the former case a larger number of virtual nodes used. Further, a comparison of Figs. 6(a) and (b) with Figs. 6(c) and (d) illustrates the reduction of connections between virtual nodes, when the fast timescale related to relaxations oscillations is damped, due to the choice of a large value for τ_L. Similarity between Fig. 6(c) and Fig. 6(d) relates

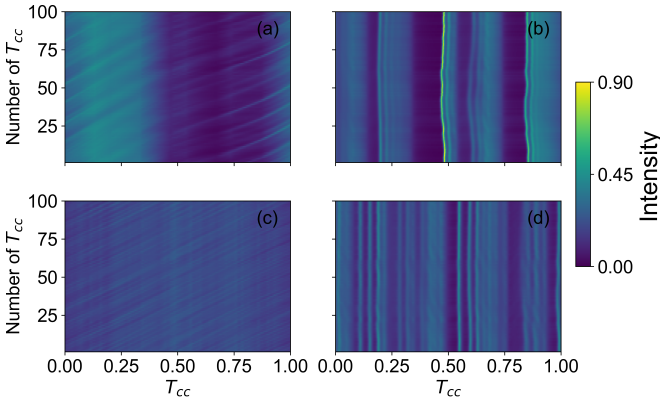

FIG. 5. 2D diagrams of the laser intensity evolution for 100 subsequent roundtrips (a), (c) outside and (b), (d) inside the resonance as indicated in Fig. 1. The diagonal features in (a) and (c) represent the connectivity between the nodes in the reservoir. The node number N is varied: (a), (b) $N = 15$, (c), (d) $N = 70$. $P = 0.2$, $\tau_L = 7.5$, $\eta = 0.98$.

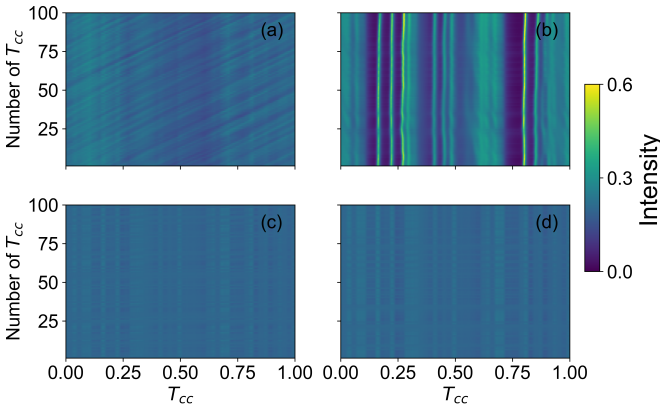

FIG. 6. 2D diagrams of the variation of τ_L. 2D diagrams of the laser intensity evolution for 100 subsequent roundtrips (a), (c) outside and (b) ,(d) inside the resonance as indicated in Fig. 3(a). The diagonal features in (a) represent the connectivity between the nodes in the reservoir. (a), (b) $\tau_L = 7.5$, (c), (d) $\tau_L = 70$. $P = 0.2$, $N = 48$, $\eta = 0.98$.

to the overall small *MC* in the case of strongly filtered feedback when the resonance is not well-pronounced (see Fig. 3). Therefore, increasing τ_L, according to the Fig. 6, leads to a loss of connectivity between some nodes as has also been discussed in the relation to the memory profiles.

IV. CONCLUSION

In this work, we have explored the resonant effects in the *MC* of a RC based on a semiconductor laser subjected to delayed optoelectronic feedback which are known to significantly affect the RC's performance. The spectral analysis revealed that the inertial and dispersive properties of eigenfrequencies define the location and width of the resonant drop in the *MC*. These properties are strongly dependant on the low-pass filter timescales τ_L and τ_H. The resonant value of the input clock time is shifted from the delay time τ due to the inertial effect and is determined by the inverse of the average interval between eigenfrequencies. Dispersive spread, corresponding to nonequidistant eigenfrequencies, lead to significant broadening of the resonant drop.

The virtual-node density of the RC affects the width of the resonant drop, but its location and the minimum *MC* value remain unaffected. We analyzed the memory function and found that while its profile changesn at the resonance, it does not depend on the number of nodes if this number is sufficiently large. At resonance, the profile consists of a fast decay indicating the loss of connectivity of some nodes, and a slow decay with the same slope as that of the memory function in the nonresonant case. The memory profile in the resonant case remains the same if the number of nodes is large, leading to a constant value of the minimum *MC*. We illustrate the change of connectivity between the virtual nodes at resonant cases by plotting 2D diagrams of the laser intensity evolution.

ACKNOWLEDGMENTS

The work of A. V. Kovalev and G. O. Danilenko was supported by the Ministry of Science and Higher Education of the Russian Federation under Grant MK-1788.2022.1.2. The work of E. A. Viktorov was supported by the Ministry of Science and Higher Education of the Russian Federation under Grant 2019-1442. D. Rontani gratefully acknowledges the support of the Chair in Photonics. E. A. Viktorov thanks the Professor@Lorraine program of LUE. D. Rontani, A. Locquet and D. S. Citrin acknowledge the support of Conseil Régional Grand Est.

[1] H. Jaeger and H. Haas, "Harnessing Nonlinearity: Predicting Chaotic Systems and Saving Energy in Wireless Communication," Science **304**, 78–80 (2004).
[2] K. Harkhoe and G. Van der Sande, "Task-independent computational abilities of semiconductor lasers with delayed optical feedback for reservoir computing," Photonics **6**, 124 (2019).
[3] M. Lukoševičius and H. Jaeger, "Reservoir computing approaches to recurrent neural network training," Computer Science Review **3**, 127–149 (2009).
[4] G. Tanaka, T. Yamane, J. B. Héroux, R. Nakane, N. Kanazawa, S. Takeda, H. Numata, D. Nakano, and A. Hirose, "Recent advances in physical reservoir computing: A review," Neural Networks **115**, 100–123 (2019).
[5] K. Nakajima and I. Fischer, eds., Reservoir Computing. Theory, Physical Implementations, (Springer, Singapore, 2021).
[6] C. Fernando and S. Sojakka, "Pattern recognition in a bucket," Lecture Notes in Artificial Intelligence (Subseries of Lecture Notes in Computer Science) **2801**, 588–597 (2003).
[7] J. C. Coulombe, M. C. York, and J. Sylvestre, "Computing with networks of nonlinear mechanical oscillators," PLoS ONE **12**, e0178663 (2017).
[8] J. Torrejon, M. Riou, F. A. Araujo, S. Tsunegi, G. Khalsa, D. Querlioz, P. Bortolotti, V. Cros, K. Yakushiji, A. Fukushima, H. Kubota, S. Yuasa, M. D. Stiles, and J. Grollier, "Neuromorphic computing with nanoscale spintronic oscillators," Nature **547**, 428–431 (2017).
[9] N. D. Haynes, M. C. Soriano, D. P. Rosin, I. Fischer, and D. J. Gauthier, "Reservoir computing with a single time-delay autonomous Boolean node," Physical Review E **91**, 020801 (2015).
[10] A. Lugnan, A. Katumba, F. Laporte, M. Freiberger, S. Sackesyn, C. Ma, E. Gooskens, J. Dambre, and P. Bienstman, "Photonic neuromorphic information processing and reservoir computing," APL Photonics **5**, 020901 (2020).

[11]D. Brunner, M. C. Soriano, and G. V. der Sande, eds., Photonic Reservoir Computing (De Gruyter, Berlin, Boston, 2019).
[12]G. Van Der Sande, D. Brunner, and M. C. Soriano, "Advances in photonic reservoir computing," Nanophotonics **6**, 561–576 (2017).
[13]L. Larger, M. C. Soriano, D. Brunner, L. Appeltant, J. M. Gutierrez, L. Pesquera, C. R. Mirasso, and I. Fischer, "Photonic information processing beyond Turing: an optoelectronic implementation of reservoir computing," Optics Express **20**, 3241–3249 (2012).
[14]Y. Chen, L. Yi, J. Ke, Z. Yang, Y. Yang, L. Huang, Q. Zhuge, and W. Hu, "Reservoir computing system with double optoelectronic feedback loops," Optics Express **27**, 27431–27440 (2019).
[15]F. Duport, A. Smerieri, A. Akrout, M. Haelterman, and S. Massar, "Fully analogue photonic reservoir computer," Scientific Reports **6**, 1–12 (2016).
[16]D. Brunner, M. C. Soriano, C. R. Mirasso, and I. Fischer, "Parallel photonic information processing at gigabyte per second data rates using transient states," Nature Communications **4**, 1364 (2013).
[17]K. Hicke, M. Escalona, D. Brunner, M. C. Soriano, I. Fischer, and C. R. Mirasso, "Information processing using transient dynamics of semiconductor lasers subject to delayed feedback," IEEE Journal of Selected Topics in Quantum Electronics **19**, 1501610 (2013).
[18]K. Vandoorne, P. Mechet, T. Van Vaerenbergh, M. Fiers, G. Morthier, D. Verstraeten, B. Schrauwen, J. Dambre, and P. Bienstman, "Experimental demonstration of reservoir computing on a silicon photonics chip," Nature Communications **5**, 3541 (2014).
[19]K. Harkhoe, G. Verschaffelt, A. Katumba, P. Bienstman, and G. Van der Sande, "Demonstrating delay-based reservoir computing using a compact photonic integrated chip," Optics Express **28**, 3086 (2020).
[20]F. D. L. Coarer, M. Sciamanna, A. Katumba, M. Freiberger, J. Dambre, P. Bienstman, and D. Rontani, "All-Optical Reservoir Computing on a Photonic Chip Using Silicon-Based Ring Resonators," IEEE Journal of Selected Topics in Quantum Electronics **24**, 7600108 (2018).
[21]J. Dong, M. Rafayelyan, F. Krzakala, and S. Gigan, "Optical Reservoir Computing Using Multiple Light Scattering for Chaotic Systems Prediction," IEEE Journal of Selected Topics in Quantum Electronics **26**, 1–12 (2019).
[22]J. Bueno, S. Maktoobi, L. Froehly, I. Fischer, M. Jacquot, L. Larger, and D. Brunner, "Reinforcement learning in a large-scale photonic recurrent neural network," Optica **5**, 756 (2018).
[23]P. Antonik, N. Marsal, D. Brunner, and D. Rontani, "Human action recognition with a large-scale brain-inspired photonic computer," Nature Machine Intelligence **1**, 530–537 (2019).
[24]L. Appeltant, M. C. Soriano, G. Van Der Sande, J. Danckaert, S. Massar, J. Dambre, B. Schrauwen, C. R. Mirasso, and I. Fischer, "Information processing using a single dynamical node as complex system," Nature Communications **2**, 468 (2011).
[25]L. Larger, A. Baylón-Fuentes, R. Martinenghi, V. S. Udaltsov, Y. K. Chembo, and M. Jacquot, "High-speed photonic reservoir computing using a time-delay-based architecture: Million words per second classification," Physical Review X **7**, 011015 (2017).
[26]Y. Paquot, F. Duport, A. Smerieri, J. Dambre, B. Schrauwen, M. Haelterman, and S. Massar, "Optoelectronic reservoir computing," Scientific reports **2**, 1–6 (2012).
[27]P. S. Dmitriev, A. V. Kovalev, A. Locquet, D. Rontani, and E. A. Viktorov, "Asymmetrical performance of a laser-based reservoir computer with optoelectronic feedback," Optics Letters **45**, 6150–6153 (2020).
[28]J. Vatin, D. Rontani, and M. Sciamanna, "Experimental reservoir computing using VCSEL polarization dynamics," Optics Express **27**, 18579 (2019).
[29]J. Bueno, J. Robertson, M. Hejda, and A. Hurtado, "Comprehensive Performance Analysis of a VCSEL-Based Photonic Reservoir Computer," IEEE Photonics Technology Letters **33**, 920–923 (2021).
[30]R. M. Nguimdo, G. Verschaffelt, J. Danckaert, and G. Van Der Sande, "Simultaneous computation of two independent tasks using reservoir computing based on a single photonic nonlinear node with optical feedback," IEEE Transactions on Neural Networks and Learning Systems **26**, 3301–3307 (2015).
[31]K. Takano, C. Sugano, M. Inubushi, K. Yoshimura, S. Sunada, K. Kanno, and A. Uchida, "Compact reservoir computing with a photonic integrated circuit," Optics Express **26**, 29424 (2018).
[32]S. Sackesyn, C. Ma, J. Dambre, and P. Bienstman, "Experimental realization of integrated photonic reservoir computing for nonlinear fiber distortion compensation," Opt. Express **29**, 30991–30997 (2021).
[33]H. Jaeger, GMD-Forschungszentrum Informationstechnik (Technical report GMD-Forschungszentrum Informationstechnik) (2002).
[34]A. Röhm and K. Lüdge, "Multiplexed networks: Reservoir computing with virtual and real nodes," Journal of Physics Communications **2**, 085007 (2018).
[35]F. Köster, D. Ehlert, and K. Lüdge, "Limitations of the Recall Capabilities in Delay-Based Reservoir Computing Systems," Cognitive Computation , 1–8 (2020).
[36]A. Röhm, L. Jaurigue, and K. Lüdge, "Reservoir computing using laser networks," IEEE Journal of Selected Topics in Quantum Electronics **26**, 7700108 (2020).
[37]F. Stelzer, A. Röhm, K. Lüdge, and S. Yanchuk, "Performance boost of time-delay reservoir computing by non-resonant clock cycle," Neural Networks **124**, 158–169 (2020).
[38]F. Köster, S. Yanchuk, and K. Lüdge, "Insight into delay based reservoir computing via eigenvalue analysis," Journal of Physics: Photonics **3**, 024011 (2021).
[39]G. O. Danilenko, A. V. Kovalev, E. A. Viktorov, A. Locquet, D. S. Citrin, and D. Rontani, "Impact of filtering on photonic time-delay reservoir computing," Chaos: An Interdisciplinary Journal of Nonlinear Science **33**, 013116 (2023).
[40]M. S. Islam, M. S. Islam, A. V. Kovalev, G. Coget, E. A. Viktorov, D. S. Citrin, D. S. Citrin, A. Locquet, and A. Locquet, "Staircase dynamics of a photonic microwave oscillator based on a laser diode with delayed optoelectronic feedback," Physical Review Applied **13**, 064038 (2020).
[41]L. Appeltant, "Reservoir computing based on delay-dynamical systems," These de Doctorat, Vrije Universiteit Brussel/Universitat de les Illes Balears (2012).
[42]L. Gonon, L. Grigoryeva, and J. P. Ortega, "Memory and forecasting capacities of nonlinear recurrent networks," Physica D: Nonlinear Phenomena **414**, 132721 (2020).
[43]S. Yanchuk and G. Giacomelli, "Spatio-temporal phenomena in complex systems with time delays," Journal of Physics A: Mathematical and Theoretical **50**, 103001 (2017).
[44]M. Yousefi, D. Lenstra, G. Vemuri, and A. Fischer, "Control of nonlinear dynamics of a semiconductor laser with filtered optical feedback," IEE Proceedings - Optoelectronics **148**, 233–237 (2001).
[45]G. Giacomelli and A. Politi, "Relationship between delayed and spatially extended dynamical systems," Phys. Rev. Lett. **76**, 2686–2689 (1996).